Bulletin of the Seismological Society of America. Vol. 54, No. 1, pp. 161–182. February, 1964

HIGHER MODE SURFACE WAVES AND THEIR BEARING ON THE STRUCTURE OF THE EARTH'S MANTLE

By Robert L. Kovach and Don L. Anderson

ABSTRACT

A detailed numerical investigation of surface wave dispersion and particle motion associated with the higher Love and Rayleigh modes over realistic earth models has been carried out as a preliminary to the routine use of these waves in studies of the crust-mantle system. The suggestion that the so-called channel waves, such as the Lg, Li, and Sa phases, can be interpreted by higher mode group velocity dispersion curves is verified in detail. Furthermore, Sa should have a higher velocity across shield areas than across normal continental areas and a higher velocity across continents than across oceans.

Higher mode Rayleigh wave data are presented for long oceanic paths to Pasadena. The observed data favor the CIT 11 model of Anderson and Toksöz (1963) over the 8099 model of Dorman *et al.* (1960) and indicate that under the Pacific Ocean the low-velocity zone extends to a depth perhaps as deep as 400 km followed by an abrupt increase in shear velocity.

Introduction

The presence of a low-velocity zone in the upper mantle has been demonstrated in various regions of the world. Observations of mantle Love and Rayleigh waves, furthermore, have indicated that the existence of a low-velocity region is a widespread phenomenon. However, a detailed picture of the low-velocity zone and of its regional variation is yet to come. Because of the inherent difficulties involved in standard body wave analyses the important questions of velocity reversals and rapid changes in velocity gradient require supplementary approaches. These difficulties are presumably most pronounced in the upper portion of the earth's mantle, in the region where surface waves have their maximum amplitude and sensitivity. To date, the surface wave data used for the study of the upper mantle have primarily been fundamental mode observations. Higher modes have not been applied to the study of this portion of the earth. There have been many observations of higher mode surface waves, but most of the previous studies (Oliver and Ewing, 1957, 1958; Kovach, 1959; Oliver, Dorman, and Sutton, 1959) were concerned with the use of higher mode data in conjunction with fundamental mode observations for the study of crustal structure and thickness.

Higher mode Love and Rayleigh wave calculations in the period range of 1 to about 50 seconds are presented for a variety of continental and oceanic models to demonstrate the behavior and sampling ability of the higher mode waves. All of the calculations have allowed for sphericity because the effect of sphericity on the higher mode dispersion curves is pronounced—particularly for earth models possessing a low-velocity zone (Kovach and Anderson, 1962). Comparison of dispersion results for equivalent spherical and flat models shows that sphericity should be considered for the higher Rayleigh modes if accurate deductions are to be made concerning the crust-mantle system.

The shape of the higher mode Love and Rayleigh wave group velocity curves is very sensitive to details of the layered wave guide. For example, the plateau structure determined for the higher modes in the Jeffreys-Bullen A model becomes

oscillatory with broad maximums and sharp minimums for a Gutenberg type velocity distribution. The higher mode curves also allow the explanation of the so-called channel waves *Lg*1, *Lg*2, *Li*, and *Sa*, as was first suggested by Oliver and Ewing (1958). Our spherical results for the successive higher mode curves for specific earth models places the higher mode explanation of "channel waves" on firm ground.

The oceanic higher mode Rayleigh wave curves are compared with new observational data in the period range of 20 to 50 seconds recorded at Pasadena. These higher mode data corroborate conclusions on oceanic mantle structure presented by Anderson *et al.* (1963).

Numerical Calculations

The method developed by Anderson and Toksöz (1963) was used to compute the dispersion of Love waves on a layered sphere. In this pseudo-spherical technique the problem of the free oscillations of a heterogeneous sphere is reformulated in

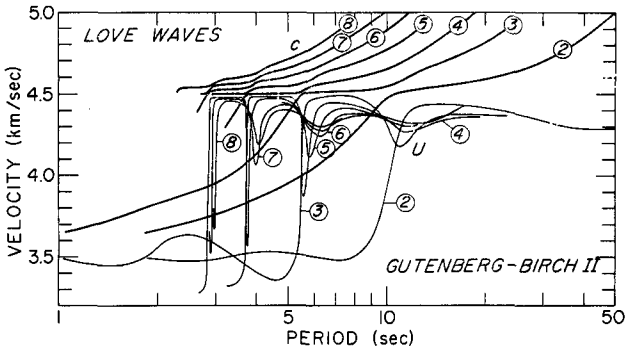

Fig. 1. First eight higher Love modes for the Gutenberg-Birch II continental model.

terms of dispersion over a plane half-space composed of anisotropic layers with a superposed velocity gradient. Group velocity is calculated exactly by the evaluation of energy integrals and by the analytical differentiation of Haskell product matrices (Harkrider and Anderson, 1963). A modified version of a torsional oscillation program (Kovach and Anderson, 1962), which allows for a liquid core and simultaneous analytic computation of group velocity during search for the eigenfrequency, was used to check by independent means the results of the pseudo-spherical calculations. The results generally agree to better than 0.06 per cent (Anderson and Toksöz, 1963).

A computer program with a double precision option (Press *et al.*, 1961) was used to compute phase and group velocities for the higher Rayleigh modes using flat layers and flat layers combined with the earth-flattening approximation (Alterman *et al.*, 1961). A program for the computation of spheroidal oscillations (Bolt and Dorman, 1961) was modified to complete double precision and used to compare results with the earth-flattening approximation. For order numbers exceeding 300 computation in double precision arithmetic is required because roundoff errors become severe in evaluation of the characteristic determinant.

DISCUSSION

Figure 1 and table 1 give dispersion results in the period range of 1 to 50 seconds for the first eight higher Love modes for the Gutenberg-Birch II model (layer parameters given in table 2) computed using spherical and pseudo-spherical techniques. Jobert (1960) first presented calculations for the first higher Love mode for a Gutenberg type spherical earth model and by extrapolation showed that a group velocity maximum of about 4.4 km/sec, appropriate in velocity for the *Sa* phase, would probably occur at a period of about 15 seconds. However, it should be emphasized that it is the group velocity plateaus in the neighborhood of 4.4 to 4.6 km/sec and the adjacent minimums for the higher modes that explain many of the observed features of *Sa* waves (Anderson and Toksöz, 1963).

TABLE 1

GUTENBERG-BIRCH II

HIGHER LOVE MODES

2nd mode			3d mode			4th mode			5th mode			6th mode		
T secs	*C* km/sec	*U* km/sec	*T* secs	*C* km/sec	*U* km/sec	*T* secs	*C* km/sec	*U* km/sec	*T* secs	*C* km/sec	*U* km/sec	*T* secs	*C* km/sec	*U* km/sec
36.53	4.800	4.305	10.11	4.550	4.286	26.74	5.340	4.389	12.41	4.900	4.308	16.87	5.361	4.421
25.36	4.650	4.378	5.52	4.500	3.959	7.84	4.600	4.436	11.30	4.840	4.306	15.84	5.291	4.394
14.62	4.550	4.440	5.26	4.450	3.480	6.19	4.565	4.406	9.48	4.75	4.363	11.63	5.000	4.326
10.57	4.500	4.139	5.06	4.400	3.404	5.64	4.530	3.880	9.01	4.73	4.380	9.75	4.880	4.357
9.16	4.400	3.648	4.87	4.350	3.370	3.75	4.500	4.283	8.52	4.710	4.395	6.31	4.680	4.245
8.24	4.300	3.525	4.68	4.300	3.357	3.71	4.490	3.478	8.26	4.700	4.402	4.83	4.600	4.449
7.38	4.200	3.488	3.84	4.100	3.427	3.69	4.485	3.450	7.46	4.670	4.411	2.32	4.520	3.374
6.50	4.100	3.491	3.64	4.061	3.459	3.68	4.480	3.433	6.93	4.650	4.399	1.58	4.420	3.202
5.54	4.000	3.515	3.30	4.000	3.520	3.65	4.470	3.410	6.45	4.630	4.343	1.23	4.410	3.177
4.49	3.900	3.533	2.57	3.900	3.628	3.53	4.420	3.352	6.10	4.610	4.206	1.00	4.400	3.170
3.38	3.800	3.506	1.81	3.800	3.489	3.48	4.400	3.340	5.98	4.600	4.138	.85	4.390	3.172
2.37	3.700	3.478	1.05	3.650	3.480	1.99	4.290	3.263	3.49	4.500	4.483	.73	4.380	3.174

The broad plateaus and the shallow and sharp minimums in the group velocity curves for periods less than 10 seconds also explain many of the observed characteristics of the *Lg* and *Li* phases. For example, the broad plateaus of 3.54 km/sec centered at a period of about 4 to 5 seconds on the second Love mode group velocity curve is appropriate both in period and velocity for many observations of *Lg*1. The fairly narrow minimum of 3.36 km/sec at a period of 4.5 seconds on the third Love mode curve is in agreement with numerous observations of the *Lg*2 phase. The extremely sharp group velocity minimums ranging from 3.58 to 3.89 km/sec are appropriate for the *Li* phase. It should be pointed out that it is probably several modes that contribute to the apparent behavior of these phases. Which modes are actually observed depends on the period range being studied and the depth of the source. Variations in the velocity and period of the *Lg* waves are observed along different paths and of course variations in the position and velocity of these maxima and minima will occur when different elastic parameters than the ones in the Gutenberg-Birch II model are used.

The relationship between the so-called channel waves and higher modes can be understood by studying plots of particle displacement versus depth. Figure 2, for example, shows displacements with depth for the fourth Love mode for the Gutenberg-Birch II model. At T = 7.37 seconds, c = 4.59 km/sec, the fourth mode group velocity curve shows a maximum of about 4.4 km/sec. Correspondingly, the two lower displacement lobes in the displacement plot are large within the low-velocity channel. As the period decreases to 5.64 seconds the group velocity dives sharply to a velocity of about 3.85 km/sec. The upper displacement lobe which was previously in the channel has now moved out of the channel and is now con-

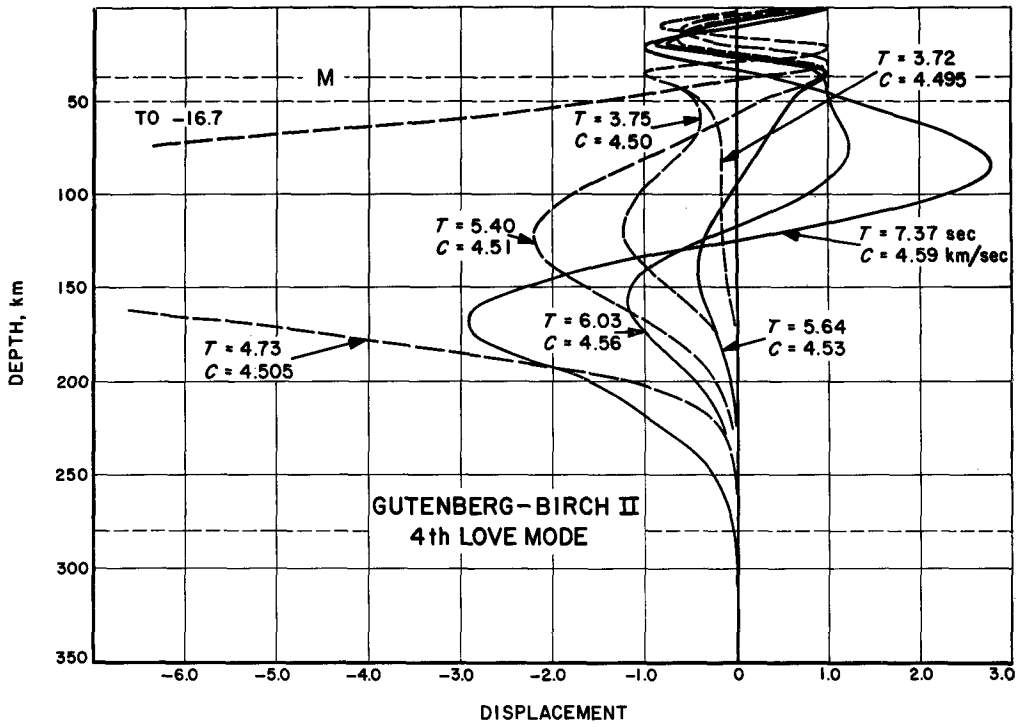

FIG. 2. Displacements with depth for the 4th Love mode, Gutenberg-Birch II model. Uncoupling from the low-velocity channel occurs when phase velocity becomes less than shear velocity of the 'lid' of the low-velocity zone.

centrated in the lower crustal layer (notice displacement curve for T = 5.64 seconds). At T = 5.40 seconds the wavelength has decreased such that the lower lobe of the displacement begins to be trapped in the channel. The group velocity curve then climbs sharply to a velocity of about 4.45 km/sec at T = 4.37 seconds. At this period the lower displacement lobe has exceedingly large amplitudes within the channel. When the period decreases to 3.72 seconds the lower displacement lobe moves out of the channel into the lower crustal layer and the group velocity curve again dives very sharply. All of these severe oscillations in the fourth Love mode group velocity curve have occurred within a small phase velocity interval, namely, 4.59 to 4.49 km/sec. Similar phenomena occur for other modes.

A characteristic behavior for the higher Love modes can thus be summarized. Oscillations in the group velocity curve occur as individual displacement lobes move in and out of the low-velocity channel. Each successively higher mode has another displacement lobe which can be trapped in the channel so that the higher mode phase velocity curves become progressively more kinky and the group velocity curves more oscillatory as the mode number is increased.

Phase and group velocity results for the first three higher Rayleigh modes, the M_{21}, the M_{12}, and the M_{22} modes (mode designation follows Tolstoy and Usdin, 1953), for the Jeffreys-Bullen A model (layer parameters taken from Sato *et al.*,

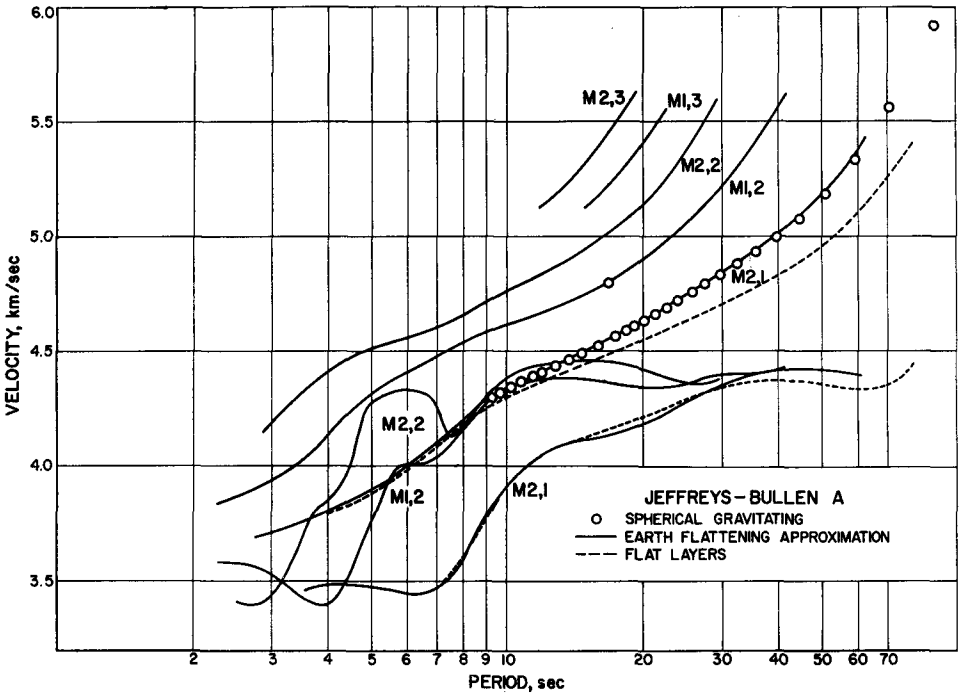

FIG. 3. Higher mode Rayleigh wave dispersion curves for the Jeffreys-Bullen A model comparing spherical, earth-flattening and plane layer calculations.

1960) are shown in figures 3 and table 2. For the M_{21} mode, phase velocities obtained from flat layer calculations combined with the earth-flattening approximation agree well with the exact spherical solution for periods less than 25 seconds. For equivalent wave periods greater than 25 seconds the phase velocities begin to diverge and the earth-flattening results are higher in phase velocity than those obtained from the spherical solution. The effect of sphericity on the M_{21} mode is surprisingly quite pronounced for wave periods down to about 8 seconds and the flat and spherical results have not merged even for periods as short as 4 seconds. However, sphericity can be neglected on the M_{21} mode group velocity curve for periods less than 30 seconds.

Figure 4 and table 3 show phase and group velocity results for the first several

TABLE 2

Order, n	T (sec)	c (km/sec)	U (km/sec)	T (sec)	U (km/sec)
	JEFFREYS-BULLEN A M_{21} *Mode* Spherical and Earth Flattening			Flat	
75	89.61	5.9170			
100	71.64	5.5601			
	61.75	5.4000	4.41	80.21	4.45
125	59.79	5.3345			
	59.20	5.3500	4.41	76.82	4.40
	56.58	5.3000	4.41	73.52	4.37
	53.90	5.2500	4.42	70.26	4.35
	51.15	5.2000	4.42	67.01	4.34
150	51.30	5.1852			
	48.32	5.1500	4.42	63.74	4.34
	45.42	5.1000	4.43	60.40	4.34
175	44.91	5.0792			
	42.47	5.0500	4.43	56.99	4.34
	39.48	5.0000	4.42	53.46	4.35
200	39.94	4.9992			
	36.48	4.9500	4.41	49.81	4.36
225	35.97	4.9350			
	33.52	4.9000	4.39	46.02	4.37
250	32.74	4.8815			
	30.65	4.8500	4.36	42.09	4.37
275	30.05	4.8354			
	27.91	4.8000	4.33	38.05	4.37
300	27.79	4.7940			
325	25.85	4.7582			
	25.36	4.7500	4.29	33.99	4.36
350	24.18	4.7226			
	23.00	4.7000	4.24	30.02	4.34
375	22.72	4.6911			
400	21.44	4.6619			
	20.84	4.6500	4.20		
425	20.30	4.6346			
450	19.28	4.6093			
	18.83	4.6000	4.17	22.97	4.26
475	18.36	4.5860			
500	17.52	4.5643			
550	16.07	4.5256			
	15.07	4.5000	4.12	17.51	4.17
600	14.84	4.4922			
650	13.79	4.4629			
	13.30	4.4500	4.09		
700	12.88	4.4366			
750	12.09	4.4123			
	11.69	4.4000	4.04	13.11	4.09
800	11.39	4.3892			
850	10.78	4.3669	3.99		
	10.35	4.3500	3.95		
900	10.23	4.3446			
950	9.74	4.3220			
	9.33	4.3000	3.83	9.95	3.97
1000	9.31	4.2989			
	8.93	4.2750	3.76		
	7.95	4.2000	3.70	8.24	3.65
	6.95	4.1000	3.47	7.13	3.49
	6.01	4.0000	3.45	6.17	3.45
	5.25	3.9250	3.47		
	3.89	3.8000	3.48	4.03	3.48
	3.05	3.7250	3.46		

T (sec)	c (km/sec)	U (km/sec)
JEFFREYS-BULLEN A M_{22} *Mode* Earth Flattening		
29.77	5.6000	4.38
28.81	5.5500	4.37
27.84	5.5000	4.37
26.86	5.4500	4.36
25.86	5.4000	4.37
24.83	5.3500	4.37
23.78	5.3000	4.38
22.69	5.2500	4.39
21.56	5.2000	4.41
20.39	5.1500	4.42
19.15	5.1000	4.44
17.87	5.0500	4.45
16.54	5.0000	4.46
15.16	4.9500	4.46
13.76	4.9000	4.46
12.35	4.8500	4.45
10.98	4.8000	4.42
9.73	4.7500	4.37
8.70	4.7000	4.27
8.27	4.6750	4.22
7.52	4.6250	4.13
6.96	4.6000	4.29
5.76	4.5500	4.33
4.75	4.5000	4.17
4.30	4.4500	3.92
4.13	4.4250	3.88
3.81	4.3750	3.82
3.42	4.3000	3.66
3.22	4.2500	3.54
3.04	4.2000	3.45
2.88	4.1500	3.41
2.55	4.0500	3.41

T (sec)	c (km/sec)	U (km/sec)
JEFFREYS-BULLEN A M_{13} *and* M_{23} *Modes* Earth Flattening		
23.09	5.5750	4.39
22.32	5.5250	4.39
21.52	5.4750	4.40
20.69	5.4250	4.42
19.84	5.3750	4.44
18.94	5.3250	4.46
18.00	5.2750	4.48
17.02	5.2250	4.49
16.00	5.1750	4.50
15.50	5.1500	4.54
18.84	5.5750	
18.16	5.5250	
17.46	5.4750	
16.73	5.4250	
15.99	5.3750	
15.25	5.3250	
14.44	5.2750	
13.57	5.2250	
12.74	5.1750	
12.35	5.1500	

TABLE 2—CONTINUED

JEFFREYS-BULLEN A M_{12} Mode Earth Flattening			GUTENBERG BIRCH II			
T (sec)	c (km/sec)	U (km/sec)	Depth (km)	α (km/sec)	β (km/sec)	ρ (g/cm^3)
41.45	5.6000	4.43	0	6.14	3.55	2.75
40.73	5.5750	4.43	19	6.14	3.55	2.75
39.32	5.5250	4.42	19	6.58	3.80	2.90
37.88	5.4750	4.41	38	6.58	3.80	2.90
36.43	5.4250	4.41	38	8.08	4.60	3.57
34.96	5.3750	4.41	60	7.87	4.51	3.51
33.46	5.3250	4.41	80	7.80	4.45	3.49
31.94	5.2750	4.40	100	7.83	4.42	3.50
30.39	5.2250	4.40	120	7.89	4.40	3.51
28.83	5.1750	4.39	140	7.94	4.39	3.53
27.26	5.1250	4.38	160	8.00	4.40	3.55
25.69	5.0750	4.37	180	8.06	4.42	3.56
24.12	5.0250	4.36	200	8.12	4.45	3.58
22.56	4.9750	4.35	220	8.20	4.48	3.61
20.98	4.9250	4.34	240	8.27	4.52	3.63
15.90	4.7750	4.37	260	8.35	4.57	3.65
14.02	4.7250	4.38	280	8.43	4.61	3.68
12.09	4.6750	4.38	300	8.51	4.66	3.70
10.27	4.6250	4.35	350	8.75	4.81	3.77
8.79	4.5750	4.25	400	9.00	4.95	3.85
7.75	4.5250	4.12	500	9.49	5.22	4.00
6.95	4.4750	4.04	550	9.74	5.36	4.07
6.25	4.4250	4.01	600	9.99	5.50	4.15
5.60	4.3750	3.96	700	10.50	5.77	4.30
4.91	4.3000	3.72	800	10.90	6.04	4.42
4.74	4.2750	3.65	900	11.30	6.30	4.54
4.45	4.2250	3.52	1000	11.40	6.35	4.57
4.20	4.1750	3.44	1200	11.80	6.50	4.69
3.97	4.1250	3.41	1400	12.05	6.60	4.77
3.74	4.0750	3.41	1600	12.30	6.75	4.85
3.49	4.0250	3.44	1800	12.55	6.85	4.92
3.37	4.0000	3.46	2000	12.80	6.95	5.00
2.73	3.9000	3.57	2200	13.00	7.00	5.06
2.32	3.8500	3.58	2400	13.20	7.10	5.12
			2600	13.45	7.20	5.19
			2800	13.70	7.25	5.27
			2898	13.65	7.20	5.25
			Mean density of core 11.03 g/cm^3.			

higher Rayleigh modes for the Gutenberg-Birch II model. A comparison of the phase velocities obtained from the exact spherical solution with those obtained from the plane layer calculations combined with the earth-flattening approximation reveals that the approximate values compare quite well with the exact spherical results for periods less than about 40 seconds. However, the flat layer phase velocity results are grossly in error down to very short periods for all of the higher modes. The disagreement is group velocity between flat and spherical calculations is not too severe for the M_{21} mode, although there is a difference in group velocity of 0.04 km/sec at a period of 11 seconds. The group velocities for the modes higher than the M_{21} mode also disagree.

In the Gutenberg-Birch II model the M_{21} mode group velocity curve has a

slight maximum of 4.34 km/sec at about 17 seconds period and a broad minimum of 4.32 km/sec centered at a period of 30 seconds. The M_{12} mode has a maximum of 4.4 km/sec at a period of 8 seconds and a fairly sharp minimum of 4.22 km/sec centered at about 20 seconds. The successively higher modes also show minimums but shifted to lower and lower periods. The low-velocity channel has a more pronounced effect on the phase velocity curves as the mode number is increased.

Higher mode calculations for the Gutenberg-Bullen A model (an earth structure similar to the Gutenberg-Birch model except that Bullen A density structure is used) are given in table 4. The M_{21} mode has a relatively broad minimum of 4.3 km/sec centered at about 35 seconds period and a group velocity maximum of about 4.4 km/sec at a period of 14 seconds. These results differ from the published results of Bolt and Dorman (1961) who found a local maximum of 4.54 km/sec at 25

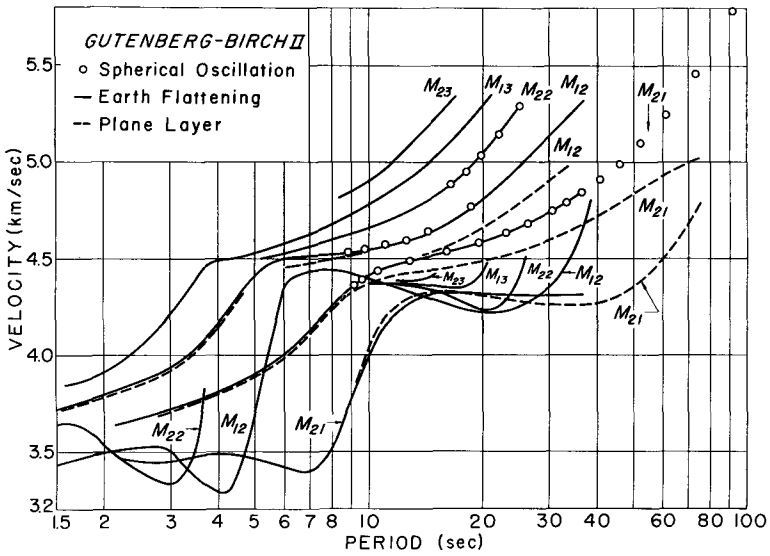

FIG. 4. Higher mode Rayleigh wave dispersion curves for the Gutenberg-Birch II model comparing spherical, earth-flattening and plane layer calculations.

seconds period and a minimum of 4.29 km/sec at 60 seconds for the M_{21} mode. For periods less than 32 seconds Bolt and Dorman's published phase velocities scatter badly and suggest machine roundoff errors.

Nevertheless, it is obvious that the local group velocity maximums for the higher Rayleigh modes can explain many of the observations of the so-called continental *Sa* wave observed on vertical component seismograms. These group velocity maximums predict a 7 to 9 second wave riding on a 14 to 25 second wave arriving with a group velocity of about 4.4 km/sec. The higher Love modes also exhibited a corresponding structure. The recording of *Sa* waves by transverse, longitudinal, and vertical component instruments can thus be easily explained by the simultaneous arrival of higher mode Love and Rayleigh waves.

Regional variations in the velocity of *Sa* should be observed. Differences in the velocity and dominant period of the transverse *Sa* wave between oceans and

TABLE 3

GUTENBERG-BIRCH II

M_{21} Mode						M_{22} Mode					
Spherical and Earth Flattening				Flat		Spherical and Earth Flattening				Flat	
Order, n	T (sec)	c (km/sec)	U (km/sec)	T (sec)	U (km/sec)	Order, n	T (sec)	c (km/sec)	U (km/sec)	T (sec)	U (km/sec)
75	91.69	5.7823					25.96	5.3210	4.51		
100	72.98	5.4581				300	25.19	5.2889			
125	60.79	5.2473					24.73	5.2710	4.38		
150	52.15	5.0998					23.62	5.2210	4.31		
		5.0210		74.73	4.78		22.58	5.1710	4.27		
175	45.70	4.9911				350	22.19	5.1466			
		4.9210		58.02	4.47		21.56	5.1210	4.24		
200	40.67	4.9085					20.53	5.0710	4.24		
225	36.65	4.8437				400	19.84	5.0386			
	36.57	4.8500	4.32				19.48	5.0210	4.25		
		4.8210		48.17	4.33		18.39	4.9710	4.26		
	33.51	4.8000	4.31			450	17.96	4.9467	4.26		
250	33.35	4.7916					17.24	4.9210	4.29		
	30.39	4.7500	4.31			500	16.37	4.8851			
275	30.60	4.7483					16.01	4.8710	4.31		
	27.21	4.7000	4.31				14.69	4.8210	4.34		
325	26.27	4.6822					13.28	4.7710	4.35		
	23.95	4.6500	4.31				11.78	4.7210	4.37		
375	23.00	4.6341					10.21	4.6710	4.37		
		4.6210		31.85	4.26		9.89	4.6610	4.37		
	20.57	4.6000	4.32				9.25	4.6410	4.32		
450	19.39	4.5825					8.66	4.6210			
	17.02	4.5500	4.33				7.93	4.6000			
550	16.03	4.5370					7.37	4.5810			
		4.5210		23.17	4.29		6.86	4.5630			
	13.51	4.5000	4.30				6.36	5.5410			
700	12.73	4.4880						4.5275		9.60	
	11.08	4.4500	4.16				5.88	4.5210			
		4.4420		14.43	4.33			4.5175		9.05	
850	10.61	4.4348						4.5075		8.51	
		4.4210		12.08	4.26		5.06	4.5000			
	9.79	4.4000	3.95	10.78	4.17			4.4975		7.96	
950	9.60	4.3887						4.4775		7.01	
1000	9.17	4.3617					3.81	4.4750			
	9.00	4.3500	3.77				3.73	4.4580			
		4.3210		8.98	3.77			4.4575		6.23	
	8.43	4.3000	3.61				3.53	4.4055	3.56		
	7.96	4.2500	3.51				3.40	4.3635	3.46		
		4.2210		7.90	3.50		3.22	4.3005	3.38		
	7.55	4.2000	3.45				2.99	4.2165	3.34		
	7.15	4.1500	3.40				2.76	4.1325	3.35		
	6.76	4.1000	3.39	6.97			2.60	4.0800	3.38		
	6.37	4.0500	3.40				2.34	4.0000	3.44		
	5.93	4.0000	3.42				2.11	3.9400	3.49		
	4.98	3.9000	3.46	5.13			1.81	3.8800	3.61		
	4.43	3.8500	3.49				1.67	3.8600	3.65		
	3.86	3.8000	3.49	4.00							
	2.78	3.7000	3.45	2.86							
	2.25	3.6500	3.46								

TABLE 3—CONTINUED

	M_{12} Mode					M_{13} and M_{23} Modes		
	Spherical and Earth Flattening			Flat		Earth Flattening		
Order, n	T (sec)	c (km/sec)	U (km/sec)	T (sec.)	U (km/sec)	T (sec.)	c (km/sec)	U (km/sec)
	38.65	5 3500	4.80			20.46	5.3210	4.48
	37.06	5.3210	4.68			18.59	5.2210	4.37
	34.84	5.2710	4.54			16.76	5.1210	4.35
	32.93	5.2210	4.45			14.86	5.0210	4.36
	31.19	5.1710	4.38			12.85	4.9210	4.37
	29.56	5.1210	4.34			10.76	4.8210	4.37
	28.00	5.0710	4.30			8.77	4.7210	
	26.47	5.0210	4.27	36.00		8.49	4.7010	
	24.97	4.9710	4.25			8.23	4.6910	
	23.49	4.9210	4.24			8.00	4.6810	
	22.02	4.8710	4.23			7.80	4.6710	
	20.53	4.8210	4.22			7.62	4.6610	
450	18.62	4.7720				7.42	4.6510	
	19.00	4.7710	4.23			7.24	4.6410	
	17.41	4.7210	4.25	22.40		7.03	4.6310	
	15.68	4.6710	4.27			6.83	4.6210	
600	14.35	4.6457				6.60	4.6110	
	13.73	4.6210	4.31			6.39	4.6010	
	13.04	4.6050	4.33			4.86	4.5270	
700	12.44	4.5946						
	12.06	4.5840	4.35			16.52	5.3220	
	10.95	4.5630	4.38			14.88	5.2220	4.42
800	10.94	4.5691				13.32	5.1220	4.39
	10.16	4.5500	4.40			11.75	5.0220	4.39
900	9.77	4.5510				10.29	4.9220	
1000	8.82	4.5361				8.39	4.8220	
		4.5220		13.94	4.24			
	7.75	4.5210	4.45					
	6.28	4.5070	4.40					
	5.85	4.4960	4.27					
	5.35	4.4570	3.94					
	4.95	4.4000	3.66					
	4.71	4.3500	3.49					
		4.3220		4.69	3.49			
	4.50	4.3000	3.38					
	4.14	4.2000	3.29					
	3.95	4.1500	3.29					
		4.1220		3.92	3.30			
	3.76	4.1000	3.32					
	3.33	4.0000	3.41					
	3.06	3.9500	3.49					
		3.9220		2.99	3.49			
	2.74	3.9000	3.53					
	2.34	3.8500	3.52					
	1.97	3.8000	3.50					
		3.7220		1.56	3.45			
	1.43	3.7000	3.43					

continents are shown in the curves of Anderson and Toksöz (1963). Brune and Dorman (1963) derived a model CANSD appropriate for the Canadian shield region. In this model the upper mantle has a high speed layer of shear velocity 4.72 km/sec down to about 115 km depth, below which the low-velocity channel has a shear velocity of about 4.5 km/sec down to a depth of 315 km. Results for the M_{21} mode for the model CANSD are given in table 5. The M_{21} mode group velocity curve shows a local maximum of 4.63 km/sec at 16 seconds period and a value of 4.43 km/sec at a period of 40 seconds. Therefore, it is probable that the velocity of *Sa* observed across shield areas will be in the range of 4.5 to 4.6 km/sec, *i.e.*, higher than across normal continental areas.

TABLE 4
GUTENBERG-BULLEN A
M_{22} *Mode*
Spherical and Earth Flattening

Order, n	T (sec)	c (km/sec)	U (km/sec)
	31.80	4.7200	4.30
	29.96	4.6950	4.30
	28.34	4.6700	4.30
	26.38	4.6450	4.31
350	24.68	4.6280	
	24.69	4.6200	4.32
400	21.74	4.5984	
	22.46	4.5950	4.33
450	19.42	4.5756	
	20.62	4.5700	4.35
	17.63	4.5450	4.38
	15.42	4.5200	4.40

TABLE 5
CANSD
M_{21} *Mode*
Spherical and Earth Flattening

Order, n	T (sec)	c (km/sec)	U (km/sec)
75	90.24	5.8753	
100	72.04	5.5293	
125	60.20	5.2988	
150	51.74	5.1411	
200	39.87	5.0073	
	28.74	4.8100	4.52
350	23.81	4.7976	
	25.78	4.7850	4.55
400	20.98	4.7639	
	23.39	4.7600	4.57
450	18.76	4.7356	
	18.78	4.7350	4.61
	15.72	4.7100	4.63
	12.83	4.6850	4.55
	10.85	4.6600	4.31
	9.78	4.6100	4.12
	9.39	4.5850	4.03
	9.03	4.5600	3.96
	8.47	4.5100	3.81

Figure 5 shows displacements with depth for the M_{21} mode for the Gutenberg-Birch II model. The maximum vertical amplitude occurs within the low-velocity channel although the amplitude is certainly not pronounced. The lack of a pronounced displacement maximum within the low-velocity zone is reflected in the group velocity structure which only shows a broad plateau and a very slight maximum at 17 seconds period. Similar particle amplitude-depth profiles for the M_{21} mode for the Gutenberg-Bullen A model show a more pronounced maximum within the low-velocity zone for the wave periods associated with the local group velocity maximum of 4.4 km/sec at 14 seconds period. The particle amplitude profiles for the Gutenberg-Birch II model also make it clear that in the period range of 10 to 90 seconds the vertical motion at the surface dominates the horizontal. Therefore, the surface motion of this phase describes a retrograde, thin vertical

ellipse. In other words, this wave appears as an SV wave travelling along the surface.

Figure 6 shows vertical displacements with depth for the M_{12} mode for the Gutenberg-Birch II model. Between 12 and 7 seconds period the lower positive lobe of the displacement has a much larger amplitude than the corresponding lobe at shorter and longer periods. Within this period interval the phase velocity ranges

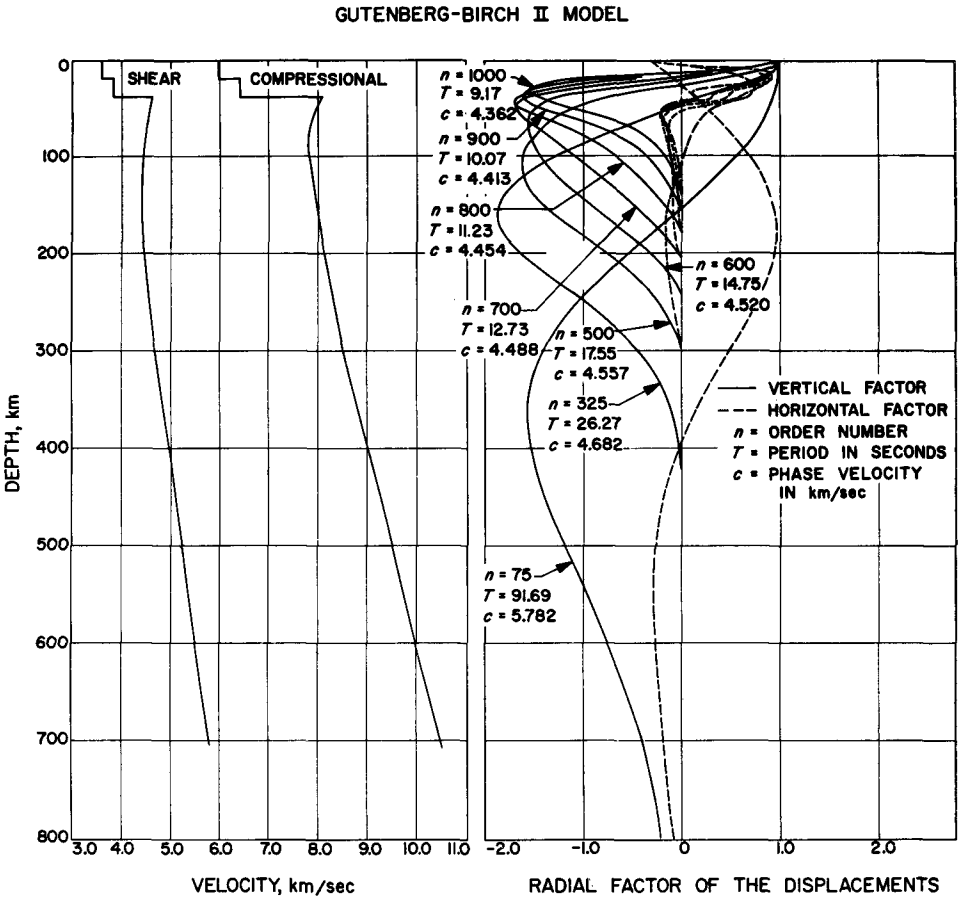

FIG. 5. Vertical and horizontal particle amplitudes with depth for the M_{21} mode (1st higher Rayleigh mode) for the Gutenberg-Birch II model. Note that the vertical displacement at the surface is much larger than the horizontal.

from about 4.55 km/sec to about 4.5 km/sec and is approximately the same as the effective shear velocity of the 'lid' of the low-velocity zone. Analogous to the behavior of the higher mode Love waves (Anderson and Toksöz, 1963) these higher mode wave periods are effectively trapped in the low-velocity zone and result in a channel wave. Uncoupling of the wave from the channel occurs when the phase velocity becomes less than the shear velocity of the lid. Figure 6 illustrates this phenomenon and shows that at a period of 5.36 seconds and a phase velocity of

4.458 km/sec the lower lobe of the vertical displacement has "popped-out" of the channel.

Horizontal displacements with depth for the M_{12} mode for the Gutenberg-Birch II model are shown in figure 7. For phase velocities greater than the shear velocity of the uncoupling zone the horizontal amplitude profiles show three nodes of motion compared to two nodes in the vertical motion. As the phase velocity approaches the velocity at which uncoupling from the channel occurs the horizontal displacement curve shows a kink associated with the uncoupling zone. The curve associated with 7.77 seconds demonstrates this behavior. When uncoupling occurs, the horizontal motion loses two nodes of motion.

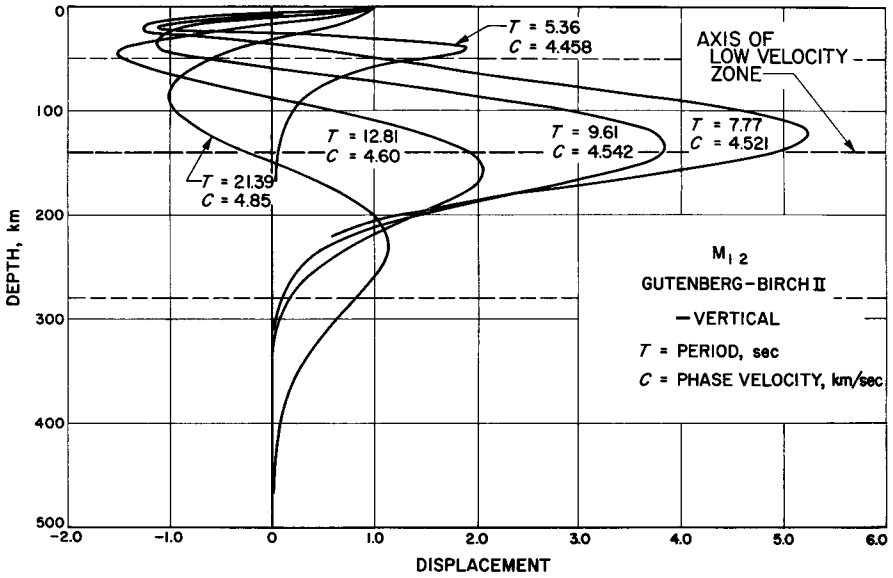

FIG. 6. Vertical particle amplitude with depth for the M_{12} mode (2nd higher Rayleigh mode) for the Gutenberg-Birch II model showing large amplitudes in the low-velocity zone. Uncoupling occurs when the phase velocity becomes less than the effective shear velocity of the lid of the low-velocity zone.

OBSERVATIONAL DATA

For long oceanic paths, waves having a pulse like or transient character in the period range of 20 to 50 seconds are frequently observed on the vertical component seismogram arriving nearly at the same time as the familiar G wave arrival on the transverse component.

Figure 8 shows long-period seismograms of the Santa Cruz Island shock of 2 January 1961 (h = 161 km; M = $6\frac{3}{4}$) recorded at Pasadena California (azimuth of approach 251°; Δ = 9476 km). The G wave arrival begins at about $10^h\ 47^m\ 00^s$ on the N–S seismogram. At this same time a pulse like wave having a period of about 26 seconds can be seen on the vertical component seismogram.

The Pasadena long-period seismograms of the Banda Sea shock of 14 February 1963 (h = 197 km; M = $6\frac{1}{2}$; Δ = 113.5°) are shown in figure 9. The great circle

path from the epicenter intersects Pasadena at an azimuth of 277° so that very little Love wave motion should be present on the *E–W* (longitudinal component) seismogram. A pronounced *G* wave arrival can be seen on the *N–S* component at about $07^h\ 52^m\ 00^s$. The *E–W* component traces are noisy but the trough at $07^h\ 52^m\ 00^s$ on the *Z* component lines up with the upward zero crossing on the *E–W* component (the vertical and longitudinal components are 90° out of phase) and

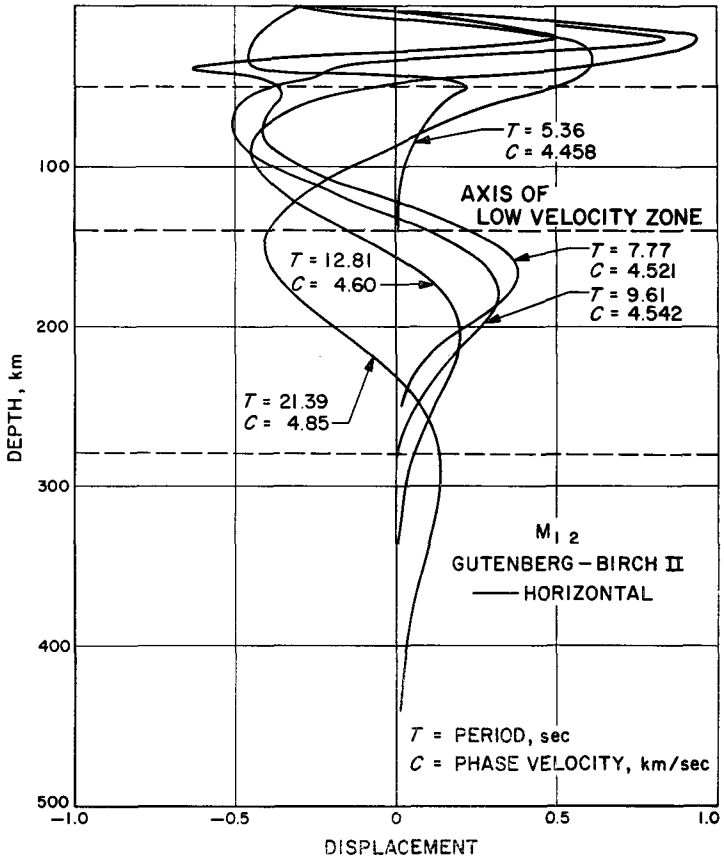

FIG. 7. Horizontal particle amplitude profiles with depth for the M_{12} mode for the Gutenberg-Birch II model. Note distortions associated with horizontal amplitude curves when uncoupling occurs.

indicates retrograde Rayleigh motion for this arrival. As a rule, however, unless the azimuth of approach is such that *G* wave motion (Love wave motion) does not contaminate the longitudinal component it is usually not possible to verify the orbital motion for Rayleigh waves in the simple visual manner. Rotation of axes can, of course, be used to generate longitudinal and transverse component seismograms of the arrival under study.

Figure 10 shows filtered vertical and longitudinal component seismograms of the Banda Sea shock described previously. A group velocity window ranging from 4.58

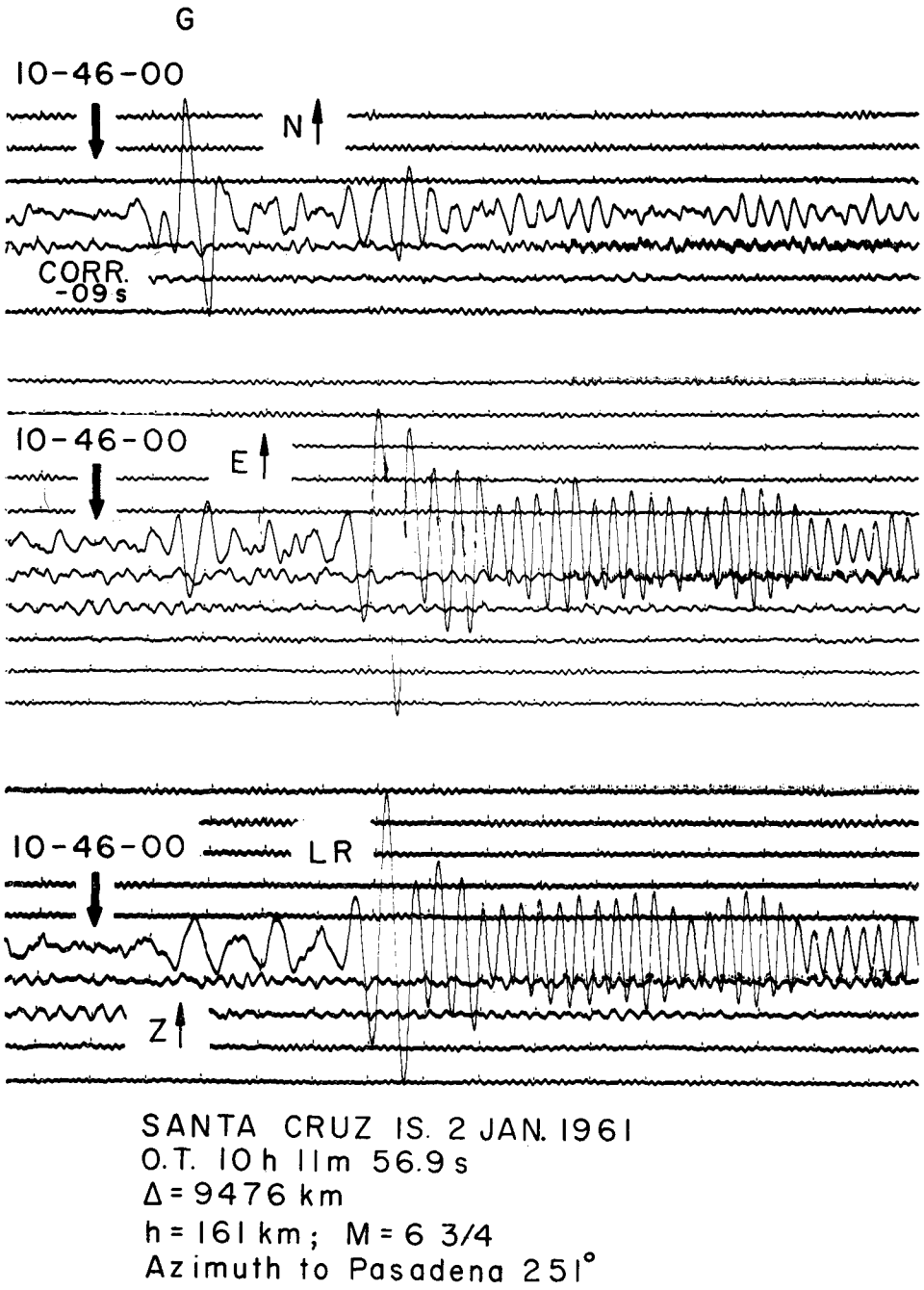

FIG. 8. Pasadena long-period seismograms (T_0 = 30 sec., T_g = 90 sec.) of the Santa Cruz Islands shock of 2 Jan 1961 showing transient arrival on Z component at same time as G wave.

km/sec to 4.3 km/sec was taken and band pass filtering in the period range of 22.5 to 27.5 seconds. Rotation of the station axes was not attempted and the vertical component and the longitudinal component are not exactly 90° out of phase but retrograde elliptical motion can be seen in the interval of 4.47 km/sec to 4.40 km/sec.

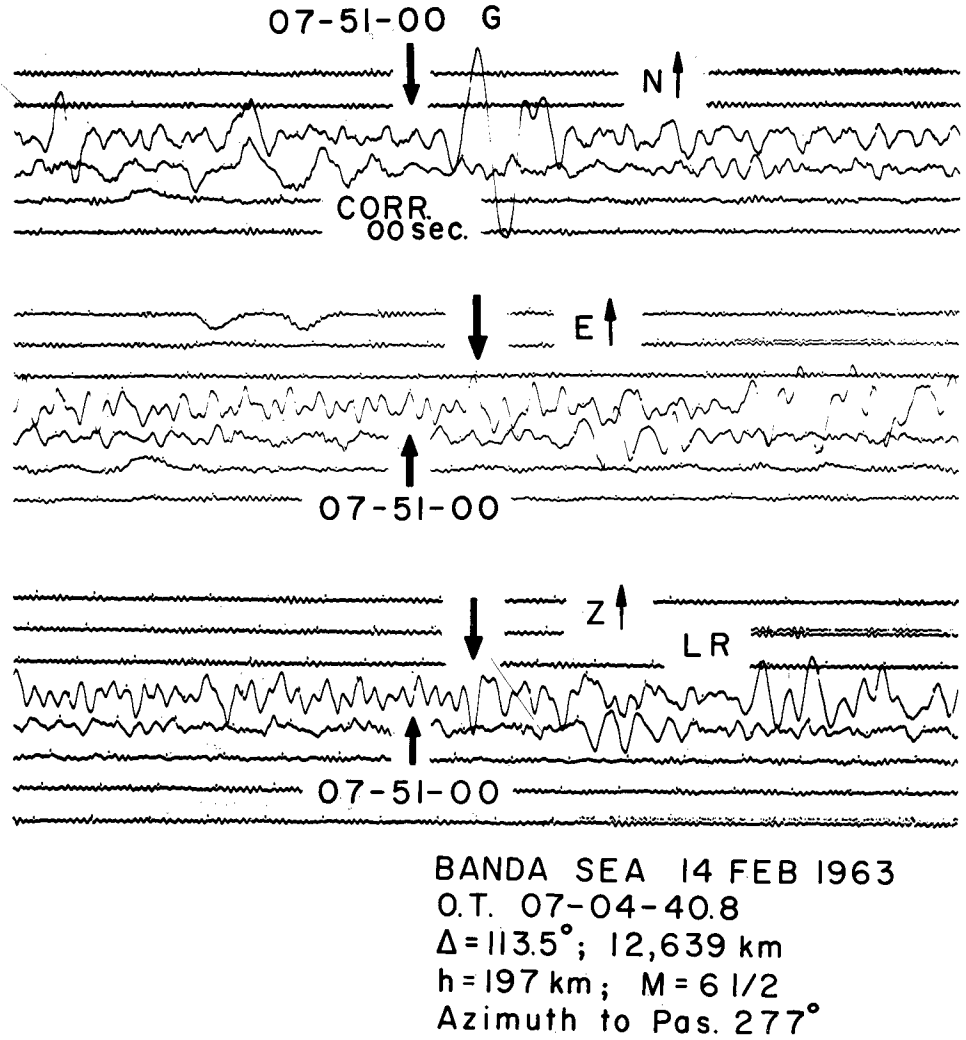

FIG. 9. Pasadena long-period seismograms (T_0 = 30 sec., T_g = 90 sec.) of Banda Sea shock of 14 Feb 1963.

Pasadena seismograms for 70 earthquakes of magnitude 6 or greater having their epicenters in the western Pacific were initially examined in search of this phase. Most all of the seismograms examined had recorded the familiar *G* wave arrival on the horizontal components. Most of the shocks studied which had a surface focus given by the USCGS or BCIS had no arrival which could be detected on the vertical component seismograms at the same time as the *G* wave on the horizontal com-

ponent seismograms. An arrival could quite commonly be found on the vertical component seismogram arriving almost or nearly simultaneously with the *G* wave, for shocks of magnitude 6 or greater having focal depths ranging from 100 to 200 kilometers.

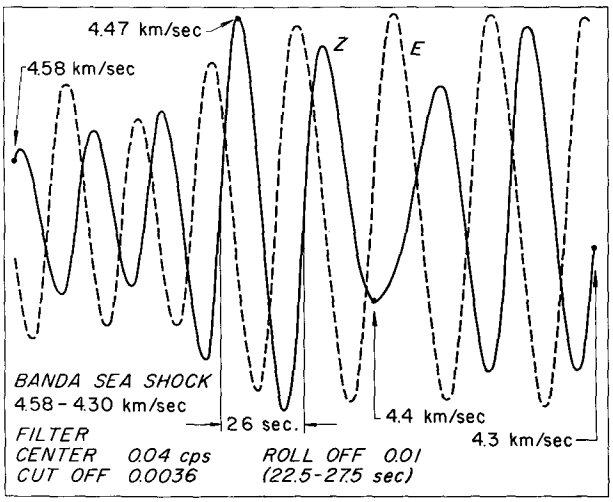

FIG. 10. Filtered seismogram of Banda Sea shock of 14 Feb 1963 showing retrograde elliptical motion in interval 4.47 to 4.4 km/sec.

TABLE 6

EARTHQUAKES IN THE PACIFIC OCEAN USED TO OBTAIN DISPERSION DATA TO PASADENA

Date	Origin Time	Location		Magnitude	Δ*°	Depth (km)
17 Dec. 1957	13h 50m 12s	12½S	166½E	7¾	85.1	100
23 Feb. 1960	16h 04m 50s	6S	154½E	6–6¼	91.1	
29 July 1960	00h 24m 06s	19½S	170½E	6½–6¾	86.3	
2 Aug. 1960	05h 07m 22.1s	22.2S	171.5E	6½	87.2	108
22 Oct. 1960	08h 22m 00.9s	10.3S	161.2E	6¾–7	88	93
2 Jan. 1961	10h 11m 56.9s	12.4S	166.4E	6¾	85.1	161
5 Jan. 1961	17h 57m 56.6s	21.2S	169.3E	6¾	88.2	123
14 Aug. 1961	23h 28m 46.5s	20.3S	169.4E	6¼	87.6	97
17 Aug. 1961	21h 16m 30s	46.3N	149.3E	6¾	67.8	186
31 May 1962	06h 28m 26.2s	22.1N	142.6E	6½	85.1	257
11 Aug. 1962	08h 15m 44s	25.2N	123.3E	6	97	140
14 Feb. 1963	07h 04m 40.8s	7.2S	128.2E	6½	113.5	197
16 Mar. 1963	08h 44m 48.3s	46.5N	154.7E	7	64.4	26

Dispersion data from the shocks listed in table 6 are compared in figure 11 with theoretical higher mode curves for two oceanic models, Case 122 and CIT 11*A*. Case 122 is a slight modification of Case 8099 of Dorman, Ewing and Oliver (1960). CIT 11A is a model, derived by successive approximations, which is compatible with oceanic mantle Love wave data (Anderson and Toksöz, 1963; Anderson *et al.*, 1963). Layer parameters for the higher mode calculations of CIT 11A are given in table 7. By analogy with the calculations presented for a Gutenberg type model, it is

assumed that for the period range under discussion the earth-flattening approximation is in close agreement with the exact spherical solution.

The M_{21} mode curve for the CIT 11A model rises steeply at a period of about 12 seconds to a velocity of about 4.35 km/sec at 15 seconds and has a broad maximum of 4.41 km/sec centered at 30 seconds period. This dispersion curve thus predicts a pulse like arrival of 20 to 40 seconds period arriving at a group velocity of about 4.4 km/sec. It is, therefore, believed that the 4.4 km/sec arrival on the vertical instruments has been propagated as the M_{21} mode, *i.e.*, the first higher Rayleigh mode. The M_{21}, the M_{12} and the M_{22} mode curves overlap in the period range from 11 to 15 seconds making mode separation and identification difficult in this period range. The M_{12} mode curve has a group velocity maximum of 4.49 km/sec at 16

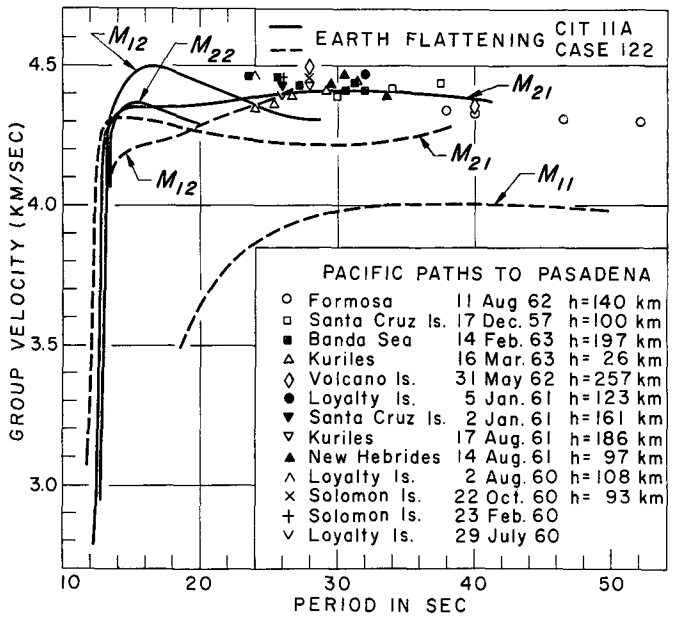

FIG. 11. Dispersion data compared with higher mode Rayleigh wave dispersion curves for two oceanic models.

seconds period and the M_{22} mode curve a maximum of 4.37 km/sec at 15 seconds period.

The oceanic model Case 122 surprisingly does not have a similar group velocity maximum for the M_{21} mode. This group velocity curve rises to a slight maximum of 4.31 km/sec at 14 seconds and then decreases to a broad minimum of 4.21 km/sec at about 28 seconds period. The M_{12} mode curve for Case 122 also does not have the necessary shape and/or velocity to predict a 4.4 km/sec pulse-like arrival. It is clear that the data favor the CIT 11A model over the Case 122 model.

Before discussing the implications of these data let us first summarize the arguments for believing that this arrival is a higher mode Rayleigh wave. (1) For the epicentral distances studied, 64 to 114 degrees, no multiple body wave arrivals could be found that were appropriate in arrival time. (2) The arrival on the vertical

component seismograms could quite commonly be found for shocks having focal depths in the range of 100 to 200 km, the depth range where 20 to 40 second M_{21} mode waves have their maximums in the vertical amplitude profiles. (3) The period and group velocity are in agreement with the theoretical dispersion curve for the M_{21} mode for the CIT 11A model. (4) When separation can be made, the arrival exhibits retrograde elliptical motion.

Vertical displacements with depth for the M_{21} mode for the CIT 11A model are presented in figure 12 together with a comparison of the velocity distributions for

TABLE 7

RAYLEIGH WAVE DISPERSION		CRUSTAL MOD OF CIT 11A	
D	ALPHA	BETA	RHO
5.00	1.5200	.0000	1.0300
.50	2.0000	.8000	1.9000
2.00	4.8000	2.8800	2.5400
5.00	6.4100	3.7000	2.9000
9.00	8.1000	4.6000	3.3200
5.00	8.1200	4.6110	3.3250
5.00	8.1200	4.6110	3.3300
10.00	8.1200	4.6090	3.3350
20.00	7.9600	4.5600	3.3500
20.00	7.7500	4.4490	3.3750
20.00	7.7000	4.3390	3.3900
20.00	7.7000	4.3400	3.4100
20.00	7.7000	4.3400	3.4250
20.00	7.8500	4.3400	3.4400
20.00	7.9500	4.5000	3.4600
20.00	8.0500	4.5000	3.4750
20.00	8.1500	4.5000	3.4900
20.00	8.2500	4.5000	3.5100
20.00	8.3500	4.5000	3.5250
20.00	8.4500	4.5000	3.5400
20.00	8.5600	4.5000	3.5600
20.00	8.6700	4.5000	3.5700
20.00	8.7800	4.5000	3.5900
20.00	8.8900	4.5000	3.6050
40.00	9.1100	4.8000	3.6300
S-INF	9.3000	5.0400	3.6900

Case 122 and CIT 11A. Case 122 (8099 mantle) has an abrupt and sharp low-velocity zone having a velocity of 4.3 km/sec in the depth interval from about 70 to about 220 km and then the velocity increases gradually with depth. On the other hand, CIT 11A has a more gradual reversal into the low-velocity zone, a slightly higher velocity in the upper channel, and a constant velocity of 4.55 km/sec in the depth interval of 160 to 360 kilometers. The low-velocity zone extends to a greater depth than in Case 122 and then the velocity increases rather sharply in the interval of 360 to 440 kilometers.

The 20 to 40 second higher mode data that we have been considering are primarily

controlled by the velocity parameters in the depth interval from about 150 to 270 kilometers. The agreement of the observed data with the model CIT 11*A*, therefore, would seem to indicate that for the long oceanic paths considered, the low-velocity zone extends to greater depths than is indicated by Case 8099 or any other proposed mantle structure. In addition, the shear velocity increases rather sharply in the depth interval of 360 to 440 kilometers. These features do not violate body wave data.

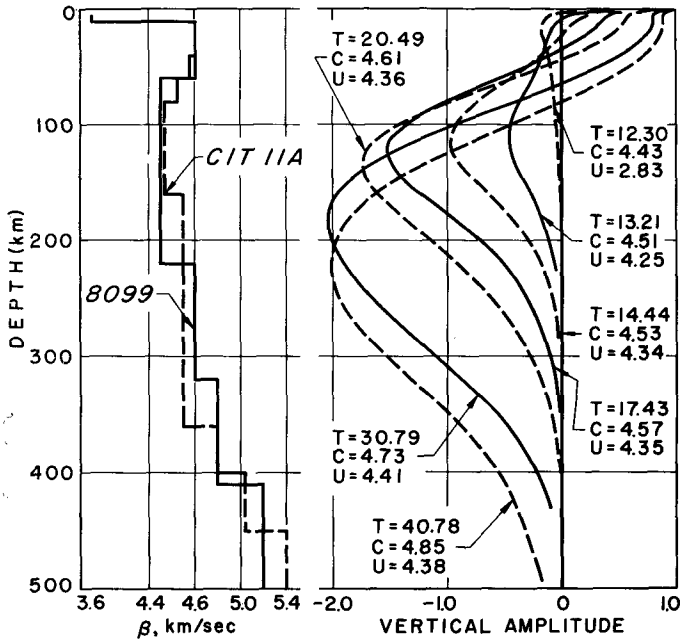

FIG. 12. Shear velocity distribution for the oceanic models CIT 11A and 8099 and vertical amplitude-depth profiles for the M_{21} mode for the model CIT 11A.

SUMMARY AND CONCLUSIONS

The broad plateaus and the shallow and sharp minimums in the higher Love mode group velocity curves can explain many of the observed characteristics of the *Lg*, *Li* and *Sa* phases.

The effect of sphericity on the higher Rayleigh modes has been found to be of great importance and to be dependent on the model under consideration. In general, the earth-flattening approximation is satisfactory for wave periods less than 25 seconds.

Calculations of the displacements with depth for the higher Rayleigh modes show a similar behavior to the higher Love modes. An effective channel wave results when the phase velocity is approximately the same as the shear velocity of the 'lid' of the low-velocity zone.

Regional variations in the velocity of *Sa* should be observed and are diagnostic of details of the upper mantle. *Sa* should have a higher velocity across shield areas compared to normal continental areas and *Sa* should have a higher velocity across continental areas than oceanic areas.

Higher mode Rayleigh wave data in the period range of 20 to 50 seconds have been observed for long oceanic paths to Pasadena and agree well with the theoretical model CIT 11A.

The model CIT 11A indicates that under the Pacific Ocean the low-velocity zone extends to greater depths (360 km) than previously indicated by the Case 8099 of Dorman, Ewing, and Oliver (1960) and that the shear velocity must increase rather abruptly in the depth interval of 360 to 440 kilometers.

Acknowledgments

This research was supported by AF-AFOSR-25-63 of the Air Force Office of Scientific Research as part of the Advanced Research Projects Agency, project VELA.

References

Alterman, Z., H. Jarosch, and C. L. Pekeris
1961. "Propagation of Rayleigh Waves in the Earth," *Geophys. J.*, 4: 219–241.

Anderson, D. L., and M. N. Toksoz
1963. "Surface Waves on a Spherical Earth 1. Upper Mantle Structure from Love Waves," *J. Geophys. Res.*, 68: 3483–3500.

Anderson, D. L., M. N. Toksoz, and R. L. Kovach
1963. "Upper Mantle Structure from Long-Period Surface Waves," presented at the *1963 International Union of Geodesy and Geophysics*, Berkeley, California.

Bolt, B., and J. Dorman
1961. "Phase and Group Velocities of Rayleigh Waves in a Spherical, Gravitating Earth, *J. Geophys. Res.*, 66: 2965–2981.

Brune, J., and J. Dorman
1963. "Seismic Waves and Earth Structure in the Canadian Shield," *Bull. Seism. Soc. Amer.*, 53: 167–210.

Dorman, J., M. Ewing, and J. Oliver
1960. "Study of Shear Velocity Distribution by Mantle Rayleigh Waves," *Bull. Seism. Soc. Amer.*, 50: 87–115.

Harkrider, D. G., and D. L. Anderson
1963. "Energy and Group Velocity of Surface Waves," unpublished manuscript.

Jobert, N.
1960. "Calcul de la dispersion des ondes de Love de grande période a la surface de la terre," *Annales de Géophysique*, 16: 393–413.

Kovach, R. L.
1959. "Surface Wave Dispersion for an Asio-African and a Eurasian Path," *J. Geophys. Res.*, 64: 805–813.

Kovach, R. L., and D. L. Anderson
1962. "Long Period Love Waves in a Heterogeneous, Spherical Earth," *J. Geophys. Res.*, 67: 5243–5255.

Oliver, J., and M. Ewing
1957. "Higher Modes of Continental Rayleigh Waves," *Bull. Seism. Soc. Amer.*, 47: 187–204.

Oliver, J., and M. Ewing
1958. "Normal Modes of Continental Surface Waves," *Bull. Seism. Soc. Amer.*, 48: 33–49.

Oliver, J., J. Dorman, and G. Sutton
1959. "The Second Shear Mode of Continental Rayleigh Waves," *Bull. Seism. Soc. Amer.*, 49: 379.

Press, F., D. Harkrider, and C. A. Seafeldt
1961. "A Fast, Convenient Program for Computation of Surface Wave Dispersion Curves in Multilayered Media," *Bull. Seism. Soc. Amer.*, 51: 495–502.

Sato, Y., M. Landisman, and M. Ewing

1960. "Love Waves in a Heterogeneous, Spherical Earth," *J. Geophys. Res.*, 65: 2395–2404.

Tolstoy, I., and Usdin, E.

1953. "Dispersive Properties of Stratified Elastic and Liquid Media: A Ray Theory," *Geophysics*, 18: 844–870.

Division of Geological Sciences
California Institute of Technology
Pasadena, California
Contribution No. 1205

Manuscript received October 14, 1963.